Heliyon 10 (2024) e31428

Contents lists available at ScienceDirect

Heliyon

journal homepage: www.cell.com/heliyon

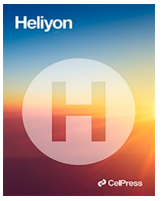

Research article

Green synthesis and characterization of polyphenol-coated magnesium-substituted manganese ferrite nanoparticles: Antibacterial and antioxidant properties

Shameran Jamal Salih [a,b,*]

[a] Department of Chemistry, Faculty of Science and Health, Koya University, Koya KOY45, Kurdistan Region – F.R., Iraq
[b] Department of Pharmaceutical Basic Sciences, Tishk International University - Erbil, Kurdistan Region, Iraq

ARTICLE INFO

Keywords:
Polyphenol
$MnFe_2O_4$
Nanomedicine
Mg-doping
Green synthesis
Antioxidant activity
Antibacterial properties

ABSTRACT

Magnesium-substituted manganese ferrite ($Mn_{0.9}Mg_{0.1}Fe_2O_4$) nanoparticles were obtained through a wet chemical method and coated with green-extracted polyphenol from Punica granatum peel. The obtained spinel nanocomposite was fully characterized. The X-ray diffraction pattern revealed a single phase with an average crystalline size of 3.33–8.74 nm, confirming the cubic-spinel structure. The FESEM micrograph showed a quasi-spherical shape with nearly uniform particles, indicating mild agglomeration. The mean size of the $Mn_{0.9}Mg_{0.1}Fe_2O_4$ was 13.66 nm with a standard deviation of 2.05. The BET isotherms indicated a surface area of 85.45 m2/g. The basic groups attached to the external surface of Mg-doped spinel ferrite were discovered. The resulted superparamagnetic modified doped-nanoferrite particles showed antibacterial activity as well as antioxidant efficiency through studying Catalase (CAT), Glutathione (GSH), and Glutathione Peroxidase (GSH-Px) parameters. The outcomes highlight the promising potential of polyphenol-functionalized $Mn_{0.9}Mg_{0.1}Fe_2O_4$ magnetite nanosized particles for the development of novel anti-biofilm agents.

1. Introduction

Magnetic nanoparticles have garnered significant interest in recent years due to their wide range of applications in various fields [1,2]. Spinel ferrites, known for their magnetic properties, magneto-optical effects, and magneto-resistive properties, have found applications in technology and medicine [3].

Ferrites primarily consist of metal oxides with iron as the predominant metallic constituent. These materials exhibit superparamagnetic behavior, making them highly useful in biomedical applications [4,5]. However, many ferrites are chemically unstable, necessitating surface modification or doping with other elements. Therefore, researchers have explored the substitution of metals such as Co, Mg, Mn, Zn, Ni, among others, to enhance the chemical stability and modify the magnetic properties of ferrites [6–9].

Among the ferrite family, $MnFe_2O_4$ has attracted significant attention due to its remarkable magnetic and electromagnetic properties [9,10]. $MnFe_2O_4$ is a partially inverse spinel, with approximately 80 % of Mn^{2+} ions occupying the tetrahedral (A) sites and the remaining 20 % in the octahedral (B) sites. Nanoparticles, nanostructures, and thin films of $MnFe_2O_4$ exhibit various characteristics, including high anisotropy constant, size-dependent saturation magnetization, superparamagnetism, and high Curie temperature.

* Corresponding author. Department of Chemistry, Faculty of Science and Health, Koya University, Koya KOY45, Kurdistan Region – F.R., Iraq.
E-mail address: shameran.jamal@koyauniversity.org.

https://doi.org/10.1016/j.heliyon.2024.e31428
Received 15 February 2024; Received in revised form 15 May 2024; Accepted 15 May 2024
Available online 16 May 2024

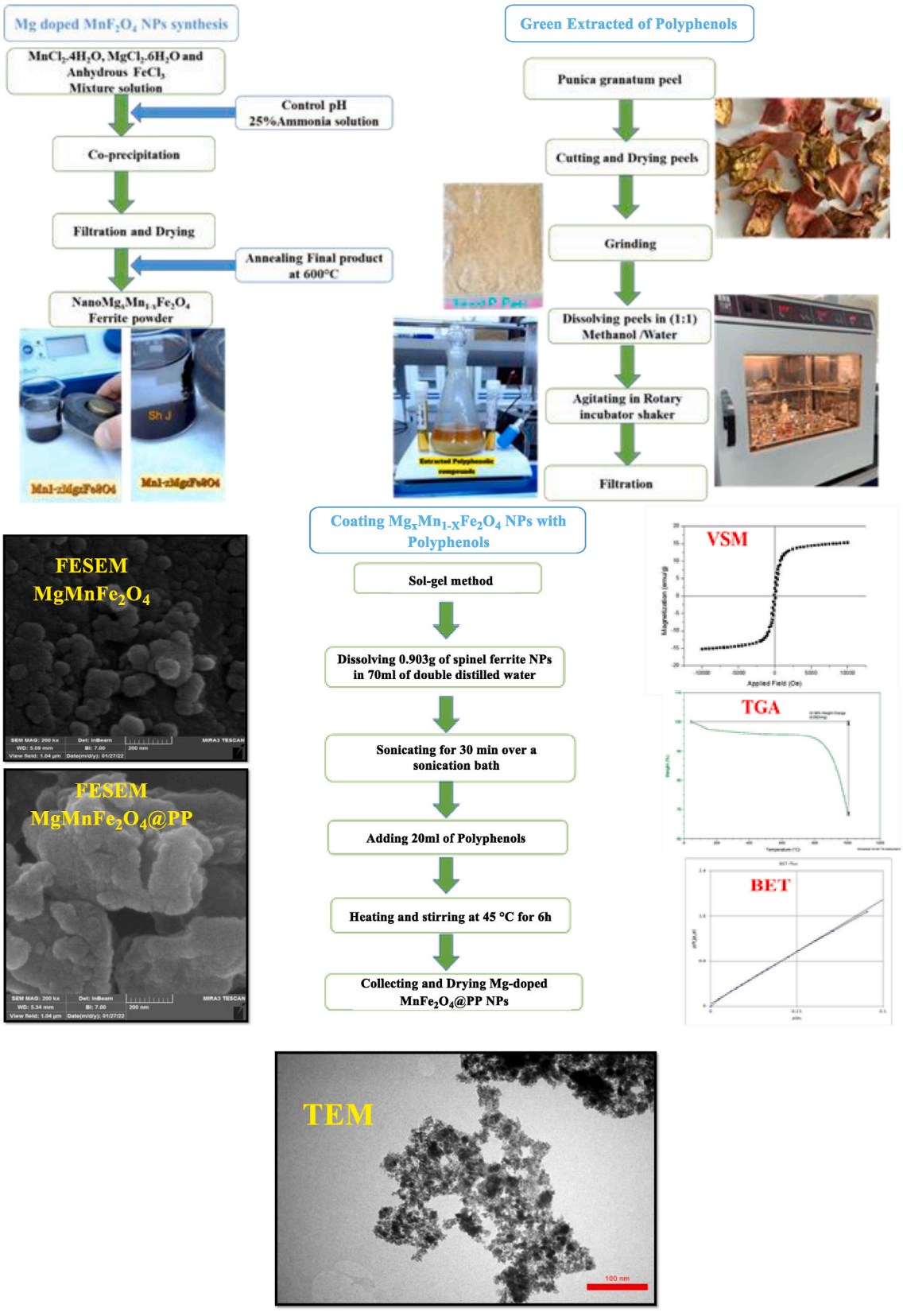

Fig. 1. Schematic diagram for the synthesis of the $Mn_{0.9}Mg_{0.1}Fe_2O_4$@PP NPs.

These unique features have led to diverse applications of $MnFe_2O_4$ NPs, such as magnetic recording, microwave technology, MRI contrast agents, Ferrofluids, site-specific drug delivery, magnetic tunnel junction-based sensors, photocatalysis, gas sensors, and absorbent materials for hot gases [11,12]. Additionally, recent studies have demonstrated the effective utilization of $MnFe_2O_4$ NPs for antibacterial and antiviral applications [13].

The properties of manganese ferrite strongly depend on its composition, morphology, and size, all of which are directly influenced by the synthesis conditions [14]. Various preparation techniques, such as hydrothermal, combustion method, co-precipitation, sol-gel, mechanochemical, solvothermal, and reverse micelle methods, have been developed for synthesizing single-domain $MnFe_2O_4$ nanoparticles [13].

The importance of using a green method in the synthesis of nanomaterials is significant because it reduces environmental impact, promotes health and safety, enhances biocompatibility, optimizes resource utilization, and offers scalability and cost-effectiveness. Green methods minimize the use of toxic chemicals, energy consumption, and waste generation, making them more environmentally friendly [15].

The application of nanotechnologies in biology has led to an increased interest in utilizing plants for the synthesis of nanoparticles, for both medical and industrial applications. Plant extracts possess reducing activity, making them suitable for the environmentally friendly production of nanoparticles. The use of biocompatible and environmentally friendly reagents in the synthesis of nanomaterials can help mitigate the adverse effects associated with the resulting materials and their by-products. In order to achieve this objective, there has been an increasing interest in the application of green synthesis, which involves the utilization of *Indian bael juice* [16], *jackfruit* extract [17], *Aegle Marmelos* extract [18], *ginger root/cardamom seeds* extract [19], and *Corchorus olitorius* [20] for the synthesis of nanoparticles. Polyphenol, a compound found in a variety of fruits, plants, and foods, has gained attention due to its wide range of biological applications [21]. It is a polyhydroxyphenolic compound with antiviral, antibacterial, and anticancer properties in various cell types [22,23].

Pseudomonas aeruginosa is a pathogenic bacterium that can cause severe diseases such as pneumonia. Gentamicin is commonly recommended as an antibiotic for treating infections caused by this bacterium and has been widely used in medical practice since the 1940s [24]. However, the increasing antimicrobial resistance rate poses a challenge, and gentamicin use is associated with toxicities like nephrotoxicity [25]. Therefore, exploring alternative approaches, such as using the synthesized nanoparticles, could be beneficial for controlling these infections.

The existing literature on manganese-based ferrite structures, particularly nanocubes (MnFe NCs), is limited. Therefore, in this study, we aimed to synthesize Mg-doped $MnFe_2O_4$ nanoparticles and then explore their potential as an antioxidant and antibacterial compound. To these purposes, we employed a novel green extraction method to obtain polyphenols from Punica granatum, which was then coated onto the as-synthesized Mg-doped $MnFe_2O_4$ nanoparticles. This coating effectively reduced the aggregation of the magnetic particles by capping them with a hydrophilic head and hydrophobic tail. Furthermore, we assessed the inhibitory mechanism of polyhydroxy phenolic compounds against Gram-negative bacteria, as well as antioxidant activity in rat model.

2. Materials and methods

2.1. Materials

All of the analytical grade reagents in this study were used as received and required no further purification. Anhydrous ferric chloride ($FeCl_3 \geq 99$ %), magnesium chloride hexahydrate ($MgCl_2.6H_2O \geq 99$ %), manganese chloride tetrahydrate ($MnCl_2.4H_2O$), and (25 %) ammonia solutions were purchased from Merk-KGaA (Darmstadt, Germany). Polyphenols including Gallic acid was extracted from Punica Granatum peel using a green extraction method. All these solutions were prepared utilizing double distilled water.

2.2. Synthesis of Mg-doped $MnFe_2O_4$ NPs

Magnesium substituted manganese ferrite nanoparticle with a chemical composition of $Mg_xMn_{1-x}Fe_2O_4$, were synthesized by a wet ferritization method utilizing stoichiometric amounts of magnesium chloride ($MgCl_2.6H_2O$, 0.01 M), manganese chloride ($MnCl_2.4H_2O$. 0.05 M), and anhydrous ferric chloride ($FeCl_3$, 0.1 M). The neutralization was conducted with ammonia solution and the pH was maintained at 11. Furthermore, the precursor salts of $MnCl_2.4H_2O$, $MgCl_2.6H_2O$, and $FeCl_3$ were dissolved separately in double distilled water (50 ml) to produce an ionic solution. A desired volume of 25 % ammonia solution was added dropwise until we reach a pH of 11. This process resulted in the formation of metal hydroxides and the subsequent formation of doped spinel ferrite $Mn_{0.9}Mg_{0.1}Fe_2O_4$ nanoparticles. The precipitate was then powdered using a mortar. Subsequently, the final product was annealed at 600 °C for 12 h, with a heating rate of 2 °C/min, to obtain a pure single-phase spinel structure. The synthesis process is represented in Fig. 1. The chemical reaction process is suggested as follows:

$$Fe^{3+} + Mn^{2+} + Mg^{2+} + 7NH_4\,OH \rightarrow \underset{\text{Formation of Metal Hydroxides}}{Fe(OH)_3 + Mn(OH)_2 + Mg(OH)_2 + 7NH_4^+}$$

$$Fe(OH)_3 \xrightarrow{[o]} \underset{\text{Ferric Oxyhydroxide}}{Fe^{3+}OOH + H_2O}$$

$$2FeOOH + Mn(OH)_2 + Mg(OH)_2 \rightarrow \text{Mg-}MnFe_2O_4 \downarrow + 3H_2O + \frac{1}{2} O_2$$

2.3. Green extracted of polyphenols

In this study, the Punica granatum peel was used as the source for extracting polyphenols. The peels were collected from the local market in Erbil, Iraq. The extraction of polyphenols from the peels involved selecting a suitable solvent to enhance its solubility. Two solvents were chosen for the extraction process including absolute methanol and a combination of methanol/Water (1:1, V/V). Methanol was selected due to its good solubility properties and can effectively extract polyphenols from the Punica granatum peel [26]. Additionally, the combination of methanol and water in equal proportions was utilized to further enhance the solubility and extraction efficiency of polyphenols. The Punica granatum peel seeds were manually separated from the peel, the separated peels were cut into small pieces and then allowed to air-dry until constant weight was obtained. The sample was homogenized utilizing a house mill until a fine powder was achieved. Then, 15 g of the powder was mixed with 50 ml of methanol (1:1) to extract polyphenols, a natural antioxidant. Further, the mixture was agitated in rotary incubator shaker (Ks 4000control, IKA) overnight. Subsequently, the supernatant was separated using syringe filter 0.2 μm. The extract was kept for further use.

2.4. Coating process

To synthesize polyphenols-coated magnesium-doped spinel ferrite ($Mn_{0.9}Mg_{0.1}Fe_2O_4$@PP) nanoparticles, the following procedure was followed: Initially, 0.903 g of spinel ferrite nanoparticles were dispersed in 70 ml of double distilled water. The dispersion was sonicated for 30 min in a sonication bath to ensure proper dispersion of the nanoparticles. Polyphenols were added slowly to the dispersion, dropwise, with a volume of 20 ml. The reaction mixture was then stirred and heated at 45 °C for 6 h at a stirring speed of 200 rpm. During the reaction, a black precipitate formed, which was collected using a permanent magnet. The $Mn_{0.9}Mg_{0.1}Fe_2O_4$@PP nanoparticles were thoroughly washed with double distilled water, followed by ethanol, for three cycles to remove any residual impurities. After washing, the nanoparticles were dried at 70 °C overnight. The dried polyphenols-coated spinel ferrite nanoparticles were then stored for further use [27].

2.5. Characterization

Various methods were employed to examine and confirm the particle size, distribution, and other relevant parameters of interest in the analysis of the as-prepared $Mn_{0.9}Mg_{0.1}Fe_2O_4$@PP. The crystalline structure of the as-prepared nano-sorbent was achieved using X-ray diffraction Philips PW1730 (Cu anode) at room temperature. The magnetic characteristics of the nanocomposite were assessed under the influence of an applied magnetic field using a MDKB vibrating sample magnetometer (VSM) at room temperature. Furthermore, the composition of the as-prepared nanocomposite was evaluated by recording infrared spectra over the range of 4000–400 cm^{-1} using a Fourier transform infrared (FTIR) spectrophotometer (Thermo avatar). Transmission electron microscopy was performed using a Philips CM120. The Field Emission Scanning Electron Microscope analysis (FESEM) was performed using a TESCAN VEGA3 model instrument. Brunauer–Emmett–Teller (BET) model and N_2 adsorption method were used to determine the specific surface area, pore volume and pore diameter were calculated measured surface area analyser BELSORP mini2. Additionally, thermogravimetric analysis (TGA) was conducted to examine the adsorbed mass of the coating and functionalization on the surface of MgCF NPs using a TA instrument, with heating from 25 °C to 1000 °C (at a rate of 10° per minute) in an argon atmosphere.

2.6. Inoculum of microorganisms

In the proposed evaluation tests, various dilutions of a fresh bacterial culture were prepared with an incubation time of less than 16 h, and these dilutions were made at low concentrations [28].

2.7. Antimicrobial susceptibility testing with antibiotics

From the bacterial exponential growth (~16 h), a cell suspension in saline was adjusted to 0.5 McFarland and inoculated in Muller Hinton Agar–MHA (Analar) using agar diffusion method [29,30]. Further, after 20 min of being allowed to stand, it was placed on the plate and incubated at 30 °C (±2) for 15–17 h. The antibiotics tested including Gentamycin, $Mn_{0.9}Mg_{0.1}Fe_2O_4$@PP (current study), Fe_3O_4@Schiff base (from previous published study was also tested on *S. aureus*). Meanwhile, bacterial susceptibility to these antibiotics was verified by measuring the diameter of the formations of inhibition zones.

2.8. In-vivo biocompatibility study

2.8.1. Animal model and experimental design

Male rats aged 13–14 weeks with a bodyweight of 210–255 g were used in an in-vivo biocompatibility study. They were kept in conventional laboratory settings, including food and water supplements. For this investigation, all of the rats were placed into three groups, each with three individuals. Control (common to all three synthesized magnetic fluids) and the synthesized magnetic fluids in

three different dosages (50 mg, 150 mg, and 350 mg/kg body weight), were injected into the rats. After 24 h, the animals were euthanized under chloroform anesthesia, and blood samples were collected for measuring antioxidant parameters using ELISA kits.

2.8.2. Biochemical parameters

Reactive oxygen species (ROS) are byproducts of oxygen metabolic (such as hydrogen peroxide and oxygen ions) that play a role in cell signaling and homeostasis. To assess the antioxidant activity of polyphenols-coated $Mn_{0.9}Mg_{0.1}Fe_2O_4$ nanoparticles, three different antioxidant parameters including Catalase (CAT), Glutathione(GSH), and Glutathione peroxidase(GPO) obtained from (Sunglong Biotech) were used to assess the antioxidant activity of $Mn_{0.9}Mg_{0.1}Fe_2O_4$@PP nanoparticles. Furthermore, the antioxidant dosages required to reduce the radicals were estimated from graphic plots for each concentration utilizing GraphPad Prism software.

2.8.3. Cytotoxicity assay

The cytotoxicity of the samples was assessed using the HeLa cell line. The cell culture medium contained 1 % penicillin-streptomycin, 0.2 % gentamycin, and 10 % fetal rat serum were employed in the medium. HeLa cells (4 *105 cells per 200 μL) were seeded in 96-well plates and cultured for 24 h in a CO_2 incubator with 5 % CO_2 at 37 °C. After incubation, the cells were filtered (using a 0.45 μm syringe filter). For each sample, duplicate wells were used, and each well received 50 ml of uncoated and coated $Mn_{0.9}Mg_{0.1}Fe_2O_4$@PP nanoparticles at a concentration of 4 mg mL^{-1}. Following that, insoluble samples were rinsed out several times with medium after 48 h of incubation [31,32]. The survival of the cells was studied using a hemocytometer and an inverted light microscope based on the following equation:

$$\%\ \text{cell viability} = \frac{\text{Total viable cells (unstained)}}{\text{Total cells (viable + dead)}} * 100 \quad \text{I}$$

3. Results and discussion

3.1. Fourier transforms infrared spectroscopy (FTIR) spectra

FTIR studies of the as-synthesized $Mn_{0.9}Mg_{0.1}Fe_2O_4$ and polyphenols-coated $Mn_{0.9}Mg_{0.1}Fe_2O_4$ was carried out at room temperature. Fig. 2a demonstrates typical spectra of naked $Mn_{0.9}Mg_{0.1}Fe_2O_4$ nanoparticles. The infrared spectra show broad metal-oxygen bands in the 1000–400 cm^{-1}. The detected band region is between 547.78 and 567.07 cm^{-1} corresponds to tetrahedral M − O stretching vibration and the band in the 460 cm^{-1} region arises from the M − O stretching vibration at the octahedral sites. The methylene (–CH_2–) group C–H symmetric and antisymmetric stretching modes are observed as a doublet band with peak maxima at 2983.88 cm^{-1} in the Mg-doped $MnFe_2O_4$ NPs sample [33]. Furthermore, Fig. 2b shows the FTIR spectrum of polyphenols-coated $Mn_{0.9}Mg_{0.1}Fe_2O_4$ nanoparticles, which was well-matched to the standard one. The O–H stretching due to the presence of a hydroxyl group and a physically adsorbed water molecule is detected at an absorption band of approximately 3400 cm^{-1}. The CH bending vibration is observed at the band around 1435.04 cm^{-1}. The symmetrical stretching of the carboxyl group is observed at the bands around 1348.24 cm^{-1}. The C–O stretching group is associated with 1064.71 cm^{-1} and C–C benzene ring vibration is associated with 861.47 cm^{-1} [34,35].

3.2. Thermogravimetric analysis

Thermal gravimetric analysis was utilized to characterize the thermal decomposition processes of polyphenols-coated $Mn_{0.9}Mg_{0.1}Fe_2O_4$ nanocomposites. Fig. 3 depicts a typical TGA graph of $Mn_{0.9}Mg_{0.1}Fe_2O_4$@PP nanocomposites.

It exhibits a total weight loss of 31.96 %. This total weight loss could be divided into multiple steps. The initial weight loss in the

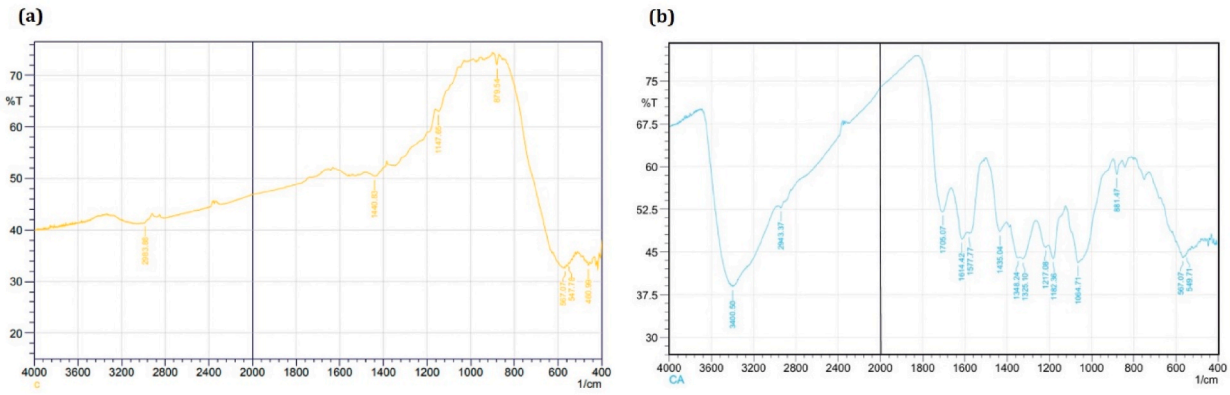

Fig. 2. FTIR spectra of (a) pure Mg-doped $MnFe_2O_4$ NPs, (b) polyphenols-coated $Mn_{0.9}Mg_{0.1}Fe_2O_4$ NPs.

first two steps is attributed to the presence of moisture contents and water molecules trapped within the pores of the prepared nanoparticles. The first weight loss is a result of the decomposition of thermally decomposable material present in the test sample. The second weight loss is caused by the sintering process of the manganese ferrite powders and the subsequent formation of the final spinel structure. The weight loss observed in the final two steps is due to the formation of metal hydroxides and their subsequent conversion into the corresponding metal oxides and ferrite nanoparticles. The TGA graph indicates an annealing temperature of 990 °C [36].

3.3. X-ray diffraction (XRD) analysis

The as-synthesized nanoparticles exhibit distinct diffraction peaks that correspond to the single spinel phase with the Fd3m space group. These peaks could be accurately indexed utilizing the following Miller indices: (111), (220), (311), (222), (400), (422), (511), (440), and (533) as shown in (Fig. 4) [37].

The prepared particles' XRD pattern reveals very broad diffraction peaks, indicating that the ferrite particles are nanosized. The average crystalline size was calculated utilizing the Debye-Scherrer equation. The average crystalline size of the synthesized nanoparticle is 6.03 nm, which falls within the range of 3.33–8.74 nm [38].

$$L = \frac{K\lambda}{\beta \cos\theta} \quad \text{I}$$

The lattice parameter corresponding to the cubic spinel structure's main (311) peak was calculated and found to be 8.3099 Å. The lattice parameters "a" of individual compositions were calculated using the following equation:

$$a = \mathrm{d}\sqrt{\mathrm{h}^2 + k^2 + l^2} \quad \text{II}$$

3.4. Brunner-Emmett-Teller (BET) surface area analysis

The porosity and N_2 adsorption-desorption measurements of the synthesized nanocomposite were measured utilizing the BET method. The method yields the pore diameter, pore volume, and surface area of the synthesized nanomaterials [39]. The BET surface area was calculated by utilizing the following equations:

$$\mathrm{Vm} = \frac{1}{slop + intercept} \quad \text{I}$$

$$\text{Total surface area} = \frac{Vm.Ns}{V} \quad \text{II}$$

$$\text{BET surface area} = \frac{S\ total}{mass\ of\ sample} \quad \text{III}$$

The BET patterns and adsorption-desorption isotherm of the prepared nanocomposites are depicted in Fig. 5A and B, respectively. The adsorption and desorption parameters of the synthesized nanomaterials are shown in Table 1. The BET graph confirms the random pore size distribution of the synthesized spinel ferrite. The substitution of elements in spinel ferrite results in larger pore diameter, volume, and surface area compared to the pure metal ferrite in its as-prepared state. The higher reactive sites to adsorb impurities from

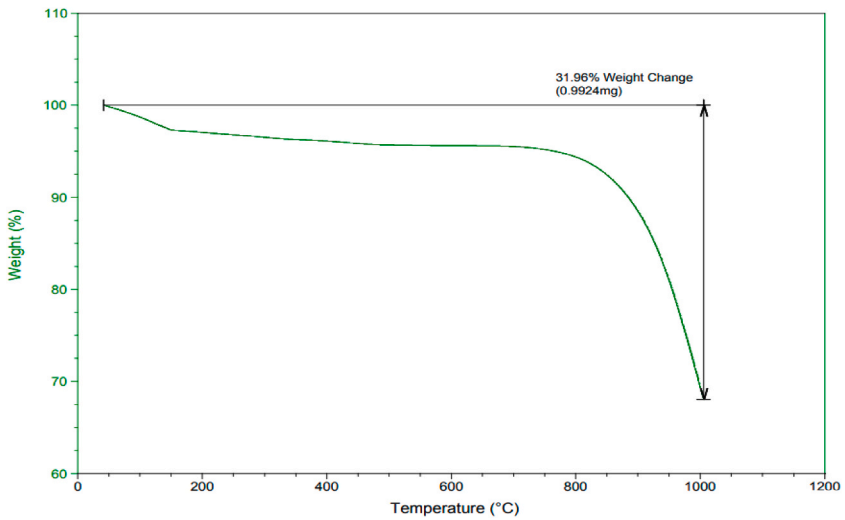

Fig. 3. TGA for $Mn_{0.9}Mg_{0.1}Fe_2O_4$@PP NPs.

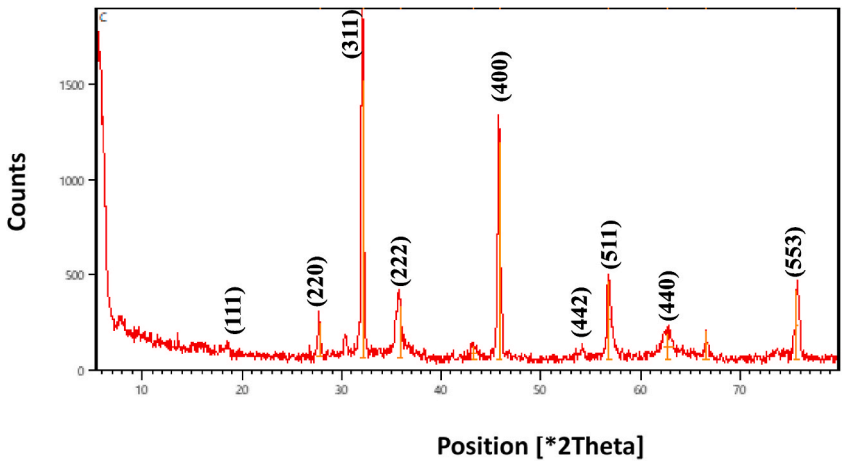

Fig. 4. XRD pattern of $Mn_{0.9}Mg_{0.1}Fe_2O_4$@PP NPs.

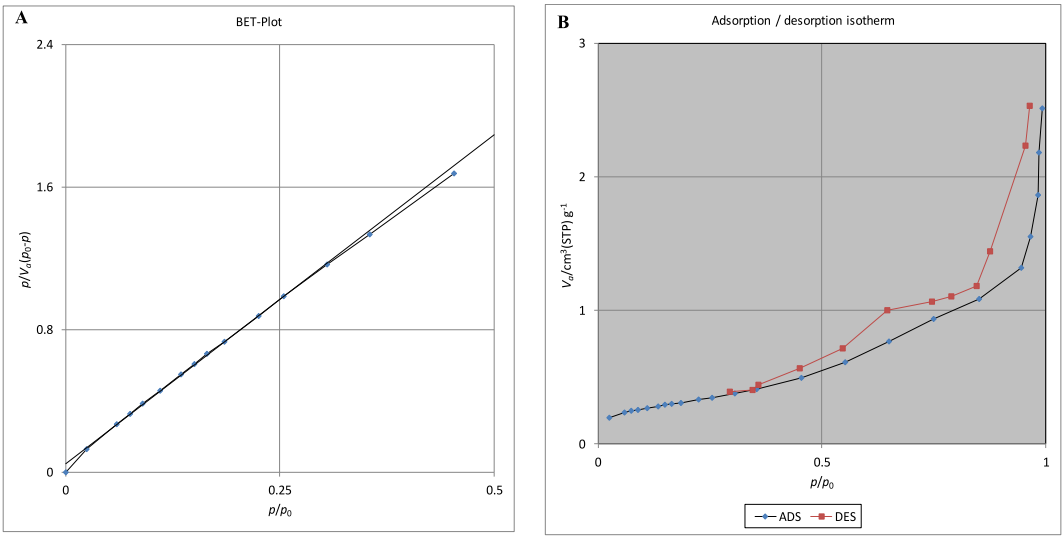

Fig. 5. BET plot (A) for polyphenols-coated $Mn_{0.9}Mg_{0.1}Fe_2O_4$ NPs and (B) adsorption-desorption isotherm.

Table 1
BET parameters for polyphenols-coated $Mn_{0.9}Mg_{0.1}Fe_2O_4$ NPs.

Sample	Surface area (M^2/g)	Pore volume ($cm^3.g^{-1}$)	Pore diameter (nm)
$Mn_{0.9}Mg_{0.1}Fe_2O_4$	85.45	0.0036695	12.628

various organic effluents were revealed by the gradual increase in surface area.

3.5. Surface properties

Morphological examinations of the as-synthesized $Mn_{0.9}Mg_{0.1}Fe_2O_4$@PP were carried out by field emission scanning electron microscopy. Fig. 6A indicates typical images of naked $Mn_{0.9}Mg_{0.1}Fe_2O_4$ nanoparticles and $Mn_{0.9}Mg_{0.1}Fe_2O_4$@PP. The micrographs demonstrate a quasi-spherical shape and nearly uniform with particles showing slight agglomeration.

Fig. 6B demonstrates a homogeneous distribution of attached polyphenols molecules that are well-dispersed on the $Mn_{0.9}Mg_{0.1}Fe_2O_4$ surface. It expresses the role of hydroxide groups working as sites for NPs heterogeneous nucleation and growth of nanoparticles. These composite materials maintain dimensions suitable for biomedical applications.

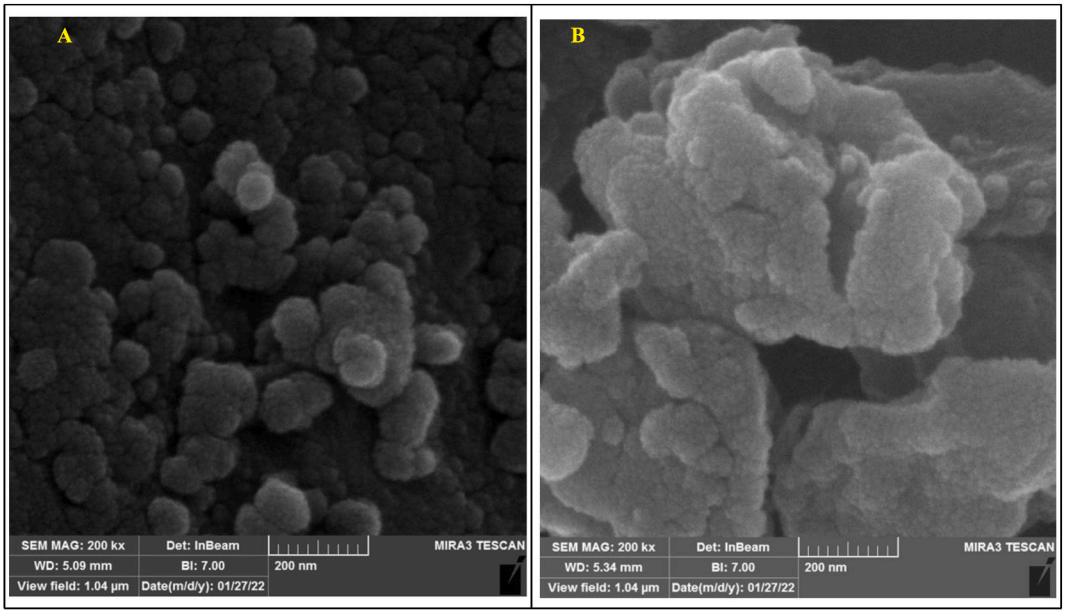

Fig. 6. FESEM images of (A) $Mn_{0.9}Mg_{0.1}Fe_2O_4$ magnetic nanoparticles, (B) $Mn_{0.9}Mg_{0.1}Fe_2O_4$ coated with polyphenols.

3.6. Energy dispersive X-ray (EDX)

The EDX reports for both $Mn_{0.9}Mg_{0.1}Fe_2O_4$ and $Mn_{0.9}Mg_{0.1}Fe_2O_4$@PP provide information on the chemical composition and potential contaminants present in the synthesized magnesium substituted manganese ferrite nanoparticles (Fig. 7a) and magnesium substituted manganese ferrite nanoparticles grafted polyphenols (Fig. 7b). The EDX results, as shown in the figures, indicate that the composition of $Mn_{0.9}Mg_{0.1}Fe_2O_4$ has the highest percentage of doped metal [40]. Additionally, Fig. 7b demonstrates the EDX spectrum which reveals the highest percentage signals of C, O, Fe, Mn and Mg, contributing to nano-ferrite structure. The highest percentage of C and O indicates the successful grafting of polyphenols onto the surface of nanostructure. Furthermore, the outcome of this study confirms that both magnesium substituted and polyphenols grafting with the manganese ferrite nanoparticles.

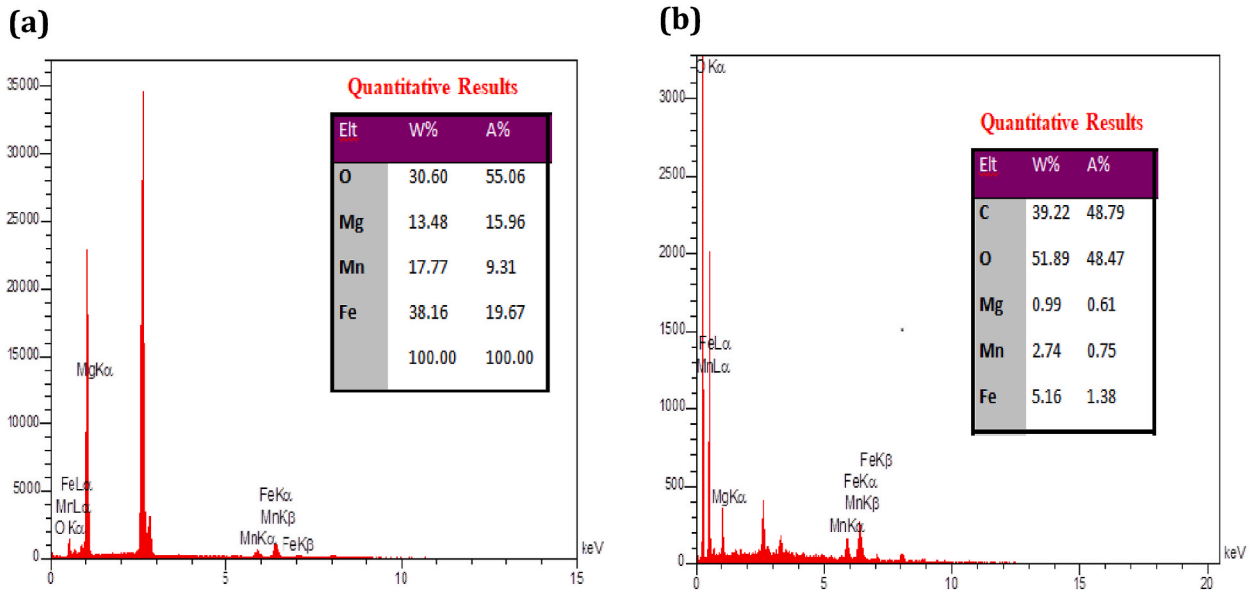

Fig. 7. The EDAX spectrum of (a) $Mn_{0.9}Mg_{0.1}Fe_2O_4$ NPs and (b) $Mn_{0.9}Mg_{0.1}Fe_2O_4$ NPs coated with polyphenols.

3.7. Evaluation of size distribution and mean size

The TEM of $Mn_{0.9}Mg_{0.1}Fe_2O_4$ nanoparticles and $Mn_{0.9}Mg_{0.1}Fe_2O_4$@PP were achieved to analysis the size, uniformity and shape of spinel structure of the particles under optimal condition (Fig. 8A,B) [41]. The histogram of the size distribution based on TEM image is demonstrated in Fig. 8C and D. The results confirm that the as-synthesized magnesium doped manganese ferrite nanoparticles exhibit a predominantly quasi-spherical shape with a narrow size distribution and very small size, averaging around 9.3 nm in diameter. In contrast, the mean size of the magnesium substituted manganese ferrite nanoparticles was found to be 13.66 nm with a standard deviation of 2.05. Moreover, the mean size of magnesium substituted manganese ferrite coated by polyphenols was 17.2 ± 2.2 nm. Consequently, the TEM results are in a good agreement with the obtained results from XRD.

3.8. Magnetic characterization using VSM

The polyphenols-coated $Mn_{0.9}Mg_{0.1}Fe_2O_4$ spinel ferrites were characterized using a vibrating sample magnetometer VSM with the range of −10,000 to 10,000 Oe as shown in Fig. 9.

The obtained values of Ms, Mr, Hc, and remanence ratio (Mr/Ms) from VSM are listed in Table 2.

Based on the obtained results, the saturation magnetization (Ms) of the pure manganese ferrite is significantly higher than that of bulk spinel ferrite. The nanocrystalline nature of the prepared samples accounts for the increase in saturation magnetization. The substitution of nonmagnetic Mg ions is responsible for the reduction in saturation magnetization. The substitution of Mg ions reduces active magnetic linkages between Fe^{2+} and Fe^{3+} ions. The decrease in magnetic interaction between the tetrahedral and octahedral sites results in a decrease in saturation magnetization. In terms of coercivity, the pure manganese ferrite sample exhibits a relatively high value compared to the bulk spinel ferrite. This higher coercivity can be attributed to the nanosized pure manganese ferrite. As the substitution of Mg in $MnFe_2O_4$ increases, the coercivity values decrease. Additionally, the substitution of nonmagnetic Mg ions also leads to a decrease in other magnetic parameters, such as the remanence magnetization (Mr). Moreover, the remanence ratio (Mr/Ms) decreases with the substitution of Mg ions in manganese ferrite [42]. Therefore, by selectively substituting tetravalent Mg^{2+} ions, the magnetic properties of $MnFe_2O_4$ nanocomposites can be tailored to suit specific applications [43,44].

3.9. Antibacterial activity of $Mn_{0.9}Mg_{0.1}Fe_2O_4$@PP

The effectiveness of $Mn_{0.9}Mg_{0.1}Fe_2O_4$@PP nanoparticles against Gram-negative bacteria, specifically *Pseudomonas aeruginosa* (as shown in Fig. 10a and b), was investigated. Various materials (listed in Table 3) were evaluated for their antibacterial properties

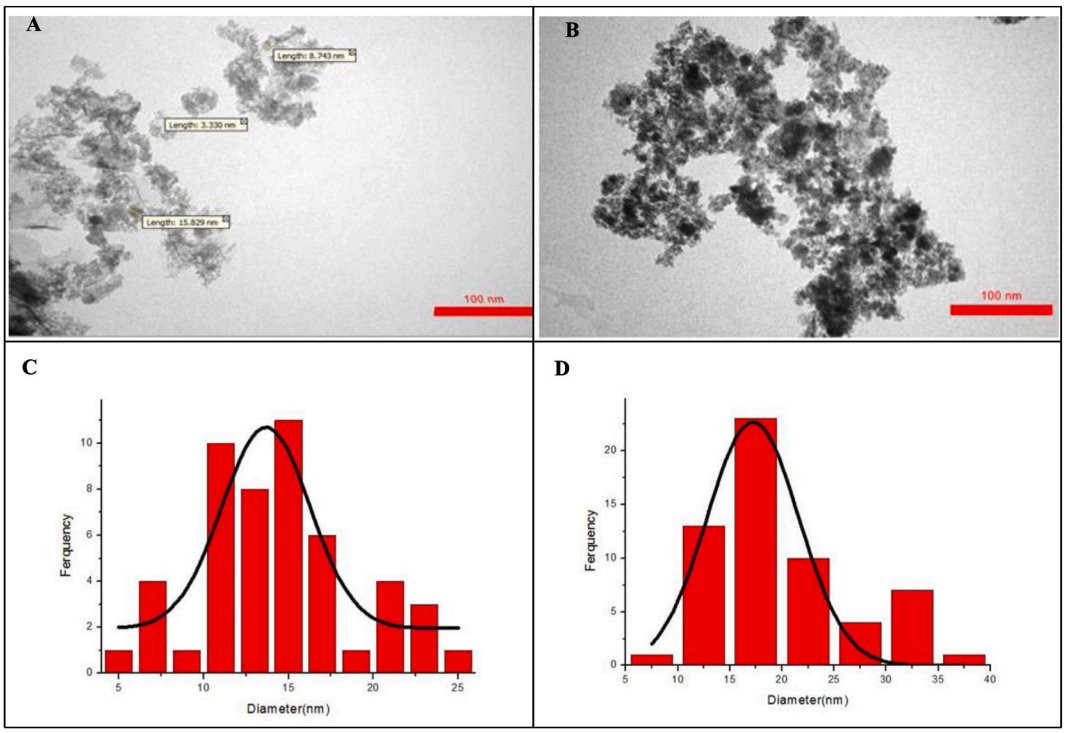

Fig. 8. TEM micrographs (**A**) for $Mn_{0.9}Mg_{0.1}Fe_2O_4$ magnetic nanoparticles with 100 nm bar, (**B**) $Mn_{0.9}Mg_{0.1}Fe_2O_4$ coated by polyphenols with 100 nm bar, (**C**) particle diameter of $Mn_{0.9}Mg_{0.1}Fe_2O_4$ nanoparticles, and (**D**) particle diameter of $Mn_{0.9}Mg_{0.1}Fe_2O_4$ nanoparticles coated with polyphenols.

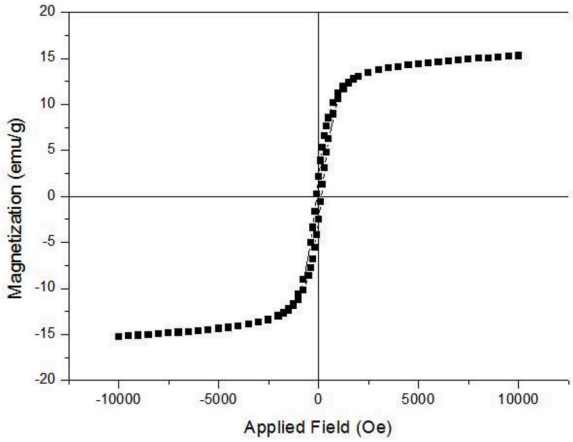

Fig. 9. Hysteresis loop of $Mn_{0.9}Mg_{0.1}Fe_2O_4$ @PP NPs.

Table 2
VSM parameters for $Mn_{0.9}Mg_{0.1}Fe_2O_4$ NPs.

Sample	Ms(emu/gm)	Mr(emu/gm)	Hc (Oe)	Mr/Ms
Mg $MnFe_2O_4$	15.2801	2.2790	−146.5743	0.1491

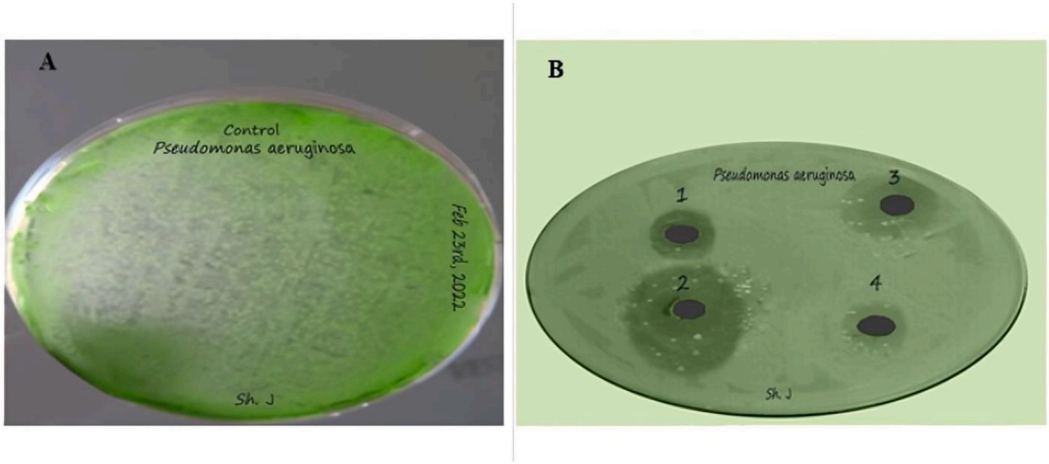

Fig. 10. Antibacterial activity of $Mn_{0.9}Mg_{0.1}Fe_2O_4$@PP for (a) control for *Pseudomonas aeruginosa*, (b) *Pseudomonas aeruginosa* [1], Gentamicin [2], $Mn_{0.9}Mg_{0.1}Fe_2O_4$@PP [3], Fe_3O_4@Schiff base [4], Amikacin.

Table 3
The diameters of the inhabitation zones for *Pseudomonas aeruginosa*.

Diameters of inhibition zone in mm				
Bacteria strain	Gentamicin	Amikacin	$Mn_{0.9}Mg_{0.1}Fe_2O_4$@PP	Fe_3O_4@Schiff base
	27	38	28	26

against *Pseudomonas aeruginosa*, and among them, $Mn_{0.9}Mg_{0.1}Fe_2O_4$@PP demonstrated the highest efficacy as an antibacterial agent. This high efficacy can be attributed to the presence of three hydroxyl groups (located in the para, ortho, and meta positions) and a carboxylic group in the main benzene ring attached to the $Mn_{0.9}Mg_{0.1}Fe_2O_4$ nanoparticles. These functional groups play a significant role in the antibacterial activity by providing a large surface area per unit mass, exhibiting magnetite behavior, and possessing other functional groups that can interact with and trap bacteria through hydrogen bonding with the amino acid side chains of the bacteria. Additionally, the hydroxyl groups in the para, ortho, and meta positions contribute to the antibacterial efficacy against *Pseudomonas aeruginosa* by forming hydrogen bonds with the peptide bond of the carbonyl group (as depicted in Fig. 10b). The antibacterial efficacy

of $Mn_{0.9}Mg_{0.}1Fe_2O_4$@PP was assessed using the diffusion method, and the growth of *Pseudomonas aeruginosa* was inhibited at a dosage of 1000 μg/ml. In contrast, the control group consisted of untreated cultures. The antibacterial efficacy was further confirmed by observing the formation of clear zones around the discs (as documented in Table 3).

3.10. *In vivo antioxidant activity*

The generation of oxidative stress in cells results from an imbalance between reactive oxygen species and excessive nitrogen production. To counteract the harmful effects of reactive species, antioxidants play a crucial role in preventing chain reactions that can damage important biological molecules and disrupt cellular processes. Antioxidants are substances that produce stable, non-reactive intermediates when exposed to further oxidation. They can be categorized into two main classes: (i) radical-trapping antioxidants, also known as chain-breaking antioxidants, which capture chain-carrying radicals and interrupt the oxidation chain; and (ii) preventive antioxidants, which decrease the rate of radical chains [45].

Catalase (CAT) is an important antioxidant enzyme found in aerobic organisms. It breaks down hydrogen peroxide into oxygen and water, and deficiencies or dysfunction in CAT are linked to various diseases, including cancer. Genetic variations in the CAT gene can also contribute to the disease development.

Glutathione (GSH) is another vital antioxidant compound that plays a significant role in defending the body against oxidative stress. It helps in the detoxification of ROS and their byproducts, such as free radicals and lipid peroxides, thereby preventing cellular damage. Imbalances in GSH homeostasis have been associated with several diseases, including neurodegenerative diseases, liver and heart disease, aging, diabetes, and cancer.

Glutathione Peroxidase (GSH-Px) is an antioxidant enzyme that relies on selenium. It is part of the enzymatic antioxidant defense system and protects cells from oxidative damage by reducing hydrogen peroxide and organic peroxides to harmless compounds using reduced glutathione. Deficiencies in GSH-Px are associated with increased levels of peroxide-related oxidants.

On the other hand, nanoparticles actively seek and eliminate free radicals, making them valuable for various medical applications.

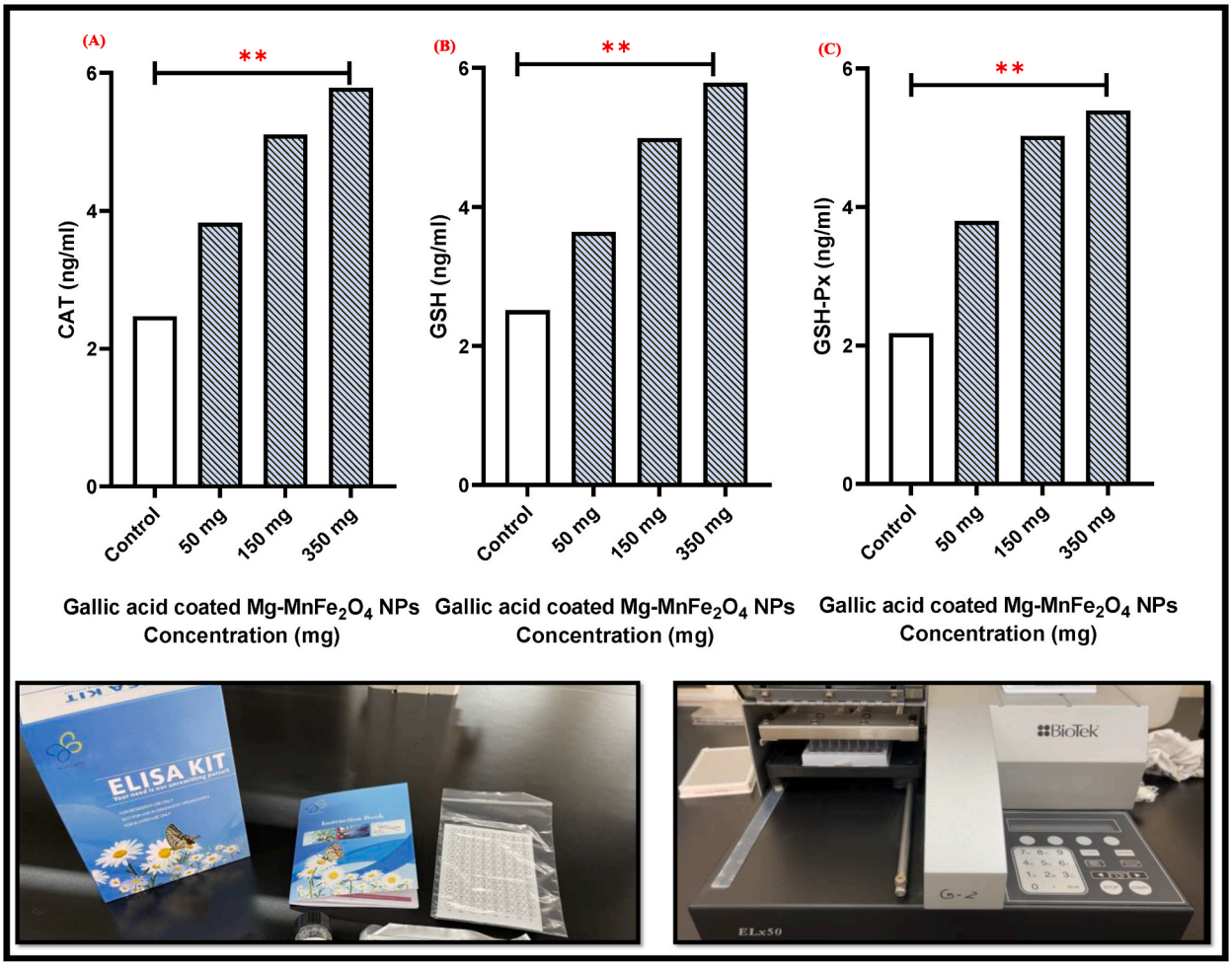

Fig. 11. Expression of biochemical parameters A) Catalase, B) Glutathione, and C) Glutathione peroxidase.

This efficacy is particularly noticeable while addressing diseases resulting from ROS that disturb the regular redox balance [46].

The antioxidant efficiency of $Mn_{0.9}Mg_{0.1}Fe_2O_4$@PP was evaluated through the parameters of CAT, GSH, and GSH-Px. Statistical analysis was conducted using analysis of variance (ANOVA), as depicted in Fig. 11A,B,C. In the study, different dosages of the synthesized nanoparticles fluid were injected into rats, with the highest influential antioxidant agents observed at a dosage of 350 mg of $Mn_{0.9}Mg_{0.1}Fe_2O_4$@PP.

4. Conclusion

The $Mn_{0.9}Mg_{0.1}Fe_2O_4$ nanoparticles coated with Polyphenols from Punica granatum peel were successfully synthesized using a wet chemical method. The nanoparticles exhibited a single-phase cubic-spinel structure with an average crystalline size of 3.33–8.74 nm. They had a quasi-spherical shape with mild agglomeration and a mean size of 13.66 nm. Notably, the polyphenols-coated $Mn_{0.9}Mg_{0.1}Fe_2O_4$ nanoparticles demonstrated antibacterial activity and antioxidant efficiency, making them promising for the development of novel anti-biofilm agents. Combining pomegranate peel extract, rich in beneficial polyphenols, with $Mn_{0.9}Mg_{0.1}Fe_2O_4$ nanoparticles offers distinct advantages. Firstly, the combination can create synergistic effects, enhancing the overall antibacterial and antioxidant properties beyond what each component can achieve alone. This can lead to improved therapeutic efficacy and a broader range of benefits. Secondly, the polyphenol coating on the nanoparticles provides a controlled release of the bioactive compounds present in the pomegranate peel extract. This controlled release mechanism ensures sustained antibacterial and antioxidant activity, enhances stability, and enables targeted delivery of the bioactive compounds to specific sites, optimizing their therapeutic effects.

Ethics approval and consent to participate

The current study was approved by the Directorate of Planning ethical committee of General Directorate of Health (Ethical code: IR. 11852).

Consent for publication

Not applicable.

Funding

No funding.

Data availability

All data generated or analyzed during this study are included in this published article [and its supplementary information files].

CRediT authorship contribution statement

Shameran Jamal Salih: Writing – original draft, Visualization, Validation, Supervision, Methodology, Investigation, Formal analysis, Conceptualization.

Declaration of competing interest

The authors declare that they have no known competing financial interests or personal relationships that could have appeared to influence the work reported in this paper.

References

[1] T. Dippong, E.A. Levei, I.G. Deac, I. Petean, O. Cadar, Dependence of structural, Morphological and magnetic properties of manganese ferrite on Ni-Mn substitution, Int. J. Mol. Sci. 23 (6) (2022) 3097.
[2] S.J. Salih, A.S.A. Kareem, S.S. Anwer, Adsorption of anionic dyes from textile wastewater utilizing raw corncob, Heliyon 8 (8) (2022) e10092.
[3] M.S.O. Pijeira, H. Viltres, J. Kozempel, M. Sakmár, M. Vlk, D. İlem-Özdemir, et al., Radiolabeled nanomaterials for biomedical applications: radiopharmacy in the era of nanotechnology, EJNMMI Radiopharmacy and Chemistry 7 (1) (2022) 1–36.
[4] M.A. Ansari, A. Baykal, S. Asiri, S. Rehman, Synthesis and characterization of antibacterial activity of spinel chromium-substituted copper ferrite nanoparticles for biomedical application, J. Inorg. Organomet. Polym. Mater. 28 (6) (2018) 2316–2327.
[5] T.N. Pham, T.Q. Huy, A.-T. Le, Spinel ferrite (AFe_2O_4)-based heterostructured designs for lithium-ion battery, environmental monitoring, and biomedical applications, RSC Adv. 10 (52) (2020) 31622–31661.
[6] T. Dippong, Characterization and Applications of Metal Ferrite Nanocomposites, Multidisciplinary Digital Publishing Institute, 2022, p. 107.
[7] H. Du, O.U. Akakuru, C. Yao, F. Yang, A. Wu, Transition metal ion-doped ferrites nanoparticles for bioimaging and cancer therapy, Translational oncology 15 (1) (2022) 101264.
[8] P.Y. Reyes-Rodríguez, D.A. Cortés-Hernández, C.A. Ávila-Orta, J. Sánchez, M. Andrade-Guel, A. Herrera-Guerrero, et al., Synthesis of Pluronic F127-coated magnesium/calcium (Mg1-xCaxFe2O4) magnetic nanoparticles for biomedical applications, J. Magn. Magn Mater. 521 (2021) 167518.
[9] S.J. Salih, L.I.A. Ali, W.M. Hamad, Novel synthesis and characterization of magnesium-doped $CoFe_2O_4$ nanoparticles–SiO_2–3-aminopropylethoxysilane– gallic acid magnetic nanocomposite for effective removal of cationic dyes, Arab. J. Chem. 17 (3) (2024) 105647.

[10] J.X. Flores-Lasluisa, D. Salinas-Torres, M.V. López-Ramón, C. Moreno-Castilla, M. Álvarez, E. Morallon, et al., Electrocatalytic activity of calcined manganese ferrite solid nanospheres in the oxygen reduction reaction, Environ. Res. 204 (2022) 112126.
[11] M.A. Njoroge, N.M. Kirimi, K.P. Kuria, Spinel ferrites gas sensors: a review of sensing parameters, mechanism and the effects of ion substitution, Crit. Rev. Solid State Mater. Sci. (2021) 1–30.
[12] J.A. Peters, Relaxivity of manganese ferrite nanoparticles, Prog. Nucl. Magn. Reson. Spectrosc. 120 (2020) 72–94.
[13] S.J. Salih, W.M. Mahmood, Review on magnetic spinel ferrite (MFe_2O_4) nanoparticles: from synthesis to application, Heliyon 9 (2023) e16601.
[14] E. Petrova, D. Kotsikau, V. Pankov, A. Fahmi, Influence of synthesis methods on structural and magnetic characteristics of Mg–Zn-ferrite nanopowders, J. Magn. Magn Mater. 473 (2019) 85–91.
[15] D. Gupta, A. Boora, A. Thakur, T.K. Gupta, Green and sustainable synthesis of nanomaterials: recent advancements and limitations, Environ. Res. 231 (2023) 116316.
[16] C. Mallikarjunaswamy, V. Lakshmi Ranganatha, R. Ramu, Nagaraju G. Udayabhanu, Facile microwave-assisted green synthesis of ZnO nanoparticles: application to photodegradation, antibacterial and antioxidant, J. Mater. Sci. Mater. Electron. 31 (2) (2020) 1004–1021.
[17] C. Mallikarjunaswamy, S. Pramila, G. Nagaraju, R. Ramu, V.L. Ranganatha, Green synthesis and evaluation of antiangiogenic, photocatalytic, and electrochemical activities of BiVO4 nanoparticles, J. Mater. Sci. Mater. Electron. 32 (10) (2021) 14028–14046.
[18] V. Lakshmi Ranganatha, S. Pramila, G. Nagaraju, Surendra BS. Udayabhanu, C. Mallikarjunaswamy, Cost-effective and green approach for the synthesis of zinc ferrite nanoparticles using Aegle Marmelos extract as a fuel: catalytic, electrochemical, and microbial applications, J. Mater. Sci. Mater. Electron. 31 (20) (2020) 17386–17403.
[19] A. Chaudhari, T. Kaida, H.B. Desai, S. Ghosh, R.P. Bhatt, A.R. Tanna, Dye degradation and antimicrobial applications of manganese ferrite nanoparticles synthesized by plant extracts, Chemical Physics Impact 5 (2022) 100098.
[20] O.H. Abd-Elkader, N.M. Deraz, L. Aleya, Corchorus olitorius-mediated green synthesis and characterization of nickel and manganese ferrite nanoparticles 15 (5) (2023) 965.
[21] H. Qin, Y. He, P. Xu, D. Huang, Z. Wang, H. Wang, et al., Spinel ferrites (MFe_2O_4): synthesis, improvement and catalytic application in environment and energy field, Adv. Colloid Interface Sci. 294 (2021) 102486.
[22] X. Sun, M. Dong, Z. Guo, H. Zhang, J. Wang, P. Jia, et al., Multifunctional chitosan-copper-gallic acid based antibacterial nanocomposite wound dressing, Int. J. Biol. Macromol. 167 (2021) 10–22.
[23] A.R. Malik, M.H. Aziz, M. Atif, M.S. Irshad, H. Ullah, T.N. Gia, et al., Lime peel extract induced $NiFe_2O_4$ NPs: synthesis to applications and oxidative stress mechanism for anticancer, antibiotic activity, J. Saudi Chem. Soc. (2022) 101422.
[24] A. Prayle, A. Watson, H. Fortnum, A. Smyth, Side effects of aminoglycosides on the kidney, ear and balance in cystic fibrosis, Thorax 65 (7) (2010) 654–658.
[25] R. Salomoni, P. Léo, A. Montemor, B. Rinaldi, M. Rodrigues, Antibacterial effect of silver nanoparticles in Pseudomonas aeruginosa, Nanotechnol. Sci. Appl. 10 (2017) 115.
[26] C.W.I. Haminiuk, M.S.V. Plata-Oviedo, A.R. Guedes, A.P. Stafussa, E. Bona, S.T. Carpes, Chemical, antioxidant and antibacterial study of Brazilian fruits, International Journal of Food Science & Technology 46 (7) (2011) 1529–1537.
[27] K. Atacan, B. Çakıroğlu, M. Özacar, Improvement of the stability and activity of immobilized trypsin on modified Fe_3O_4 magnetic nanoparticles for hydrolysis of bovine serum albumin and its application in the bovine milk, Food Chem. 212 (2016) 460–468.
[28] G. Agarwal, A. Kapil, S.K. Kabra, B.K. Das, S.N. Dwivedi, Characterization of Pseudomonas aeruginosa isolated from chronically infected children with cystic fibrosis in India, BMC Microbiol. 5 (1) (2005) 1–11.
[29] S.J. Salih, A.K. Smail, Synthesis, characterization and evaluation of antibacterial efficacy of zinc oxide nanoparticles, Pharmaceutical and biological evaluations 3 (3) (2016) 327–333.
[30] E. Fantozzi, E. Rama, C. Calvio, B. Albini, P. Galinetto, M. Bini, Silver doped magnesium ferrite nanoparticles: physico-chemical characterization and antibacterial activity, Materials 14 (11) (2021) 2859.
[31] S. Kanagesan, M. Hashim, S. AB Aziz, I. Ismail, S. Tamilselvan, N.B. Alitheen, et al., Evaluation of antioxidant and cytotoxicity activities of copper ferrite ($CuFe_2O_4$) and zinc ferrite ($ZnFe_2O_4$) nanoparticles synthesized by sol-gel self-combustion method, Appl. Sci. 6 (9) (2016) 184.
[32] M.A. Islam, M.R. Hasan, M.M. Haque, R. Rashid, I.M. Syed, S.M. Hoque, Efficacy of surface-functionalized $Mg_{1-x}Co_xFe_2O_4$ ($0 \leq x \leq 1$; $\Delta x = 0.1$) for hyperthermia and in vivo MR imaging as a contrast agent, RSC Adv. 12 (13) (2022) 7835–7849.
[33] M.A. Yousuf, M.M. Baig, N.F. Al-Khalli, M.A. Khan, M.F.A. Aboud, I. Shakir, et al., The impact of yttrium cations (Y^{3+}) on structural, spectral and dielectric properties of spinel manganese ferrite nanoparticles, Ceram. Int. 45 (8) (2019) 10936–10942.
[34] A. Sharma, K.M. Batoo, O.M. Aldossary, S. Jindal, N. Aggarwal, G. Kumar, Investigation of dielectric, electrical and optical properties of copper substituted Mn-Zn nanoferrites, J. Mater. Sci. Mater. Electron. 32 (1) (2021) 313–322.
[35] A. El-Denglawey, V.J. Angadi, K. Manjunatha, B. Chethan, S.B. Somvanshi, Role of dysprosium in enhancing the humidity sensing performance in manganese zinc ferrites for sensor applications, J. Mater. Sci. Mater. Electron. 32 (18) (2021) 23554–23565.
[36] S. Nazir, S. Sami, S. Haider, M. Shahid, M. Sher, M.F. Warsi, et al., Structural, spectral, dielectric and photocatalytic studies of Zr-Ni doped $MnFe_2O_4$ co-precipitated nanoparticles, Ceram. Int. 42 (12) (2016) 13459–13463.
[37] S. Keerthana, R. Yuvakkumar, P.S. Kumar, G. Ravi, D. Velauthapillai, Rare earth metal (Sm) doped zinc ferrite ($ZnFe_2O_4$) for improved photocatalytic elimination of toxic dye from aquatic system, Environ. Res. 197 (2021) 111047.
[38] A. Kumar, N. Yadav, D.S. Rana, P. Kumar, M. Arora, R. Pant, Structural and magnetic studies of the nickel doped $CoFe_2O_4$ ferrite nanoparticles synthesized by the chemical co-precipitation method, J. Magn. Magn Mater. 394 (2015) 379–384.
[39] A. Almahri, The solid-state synthetic performance of bentonite stacked manganese ferrite nanoparticles: adsorption and photo-fenton degradation of MB dye and antibacterial applications, J. Mater. Res. Technol. 17 (2022) 2935–2949.
[40] Y. Sandeep, T. Rambabu, G. Vinod, M.V. Narayana, G. Aravind, V. Nathanial, Investigation of structural and dielectric properties of Gd^{3+} substituted nickel-zinc ferrite prepared via low-temperature citrate gel self-ignited process, Mater. Today Proc. 59 (2022) 1211–1220.
[41] I. Chihi, M. Baazaoui, N. Hamdaoui, J. Greneche, M. Oumezzine, K. Farah, Sol–gel synthesis and characterization of magnesium ferrites by XRD, TEM, EPR, Mossbauer, and impedance spectroscopy, J. Mater. Sci. Mater. Electron. 32 (12) (2021) 16634–16647.
[42] M.P. Ghosh, S. Mukherjee, Disordered surface spins induced large exchange anisotropy in single-phase Sm^{3+} ions substituted nickel ferrite nanoparticles, J. Magn. Magn Mater. 489 (2019) 165320.
[43] Y. Ahmad, B. Raina, S. Thakur, K. Bamzai, Magnesium and yttrium doped superparamagnetic manganese ferrite nanoparticles for magnetic and microwave applications, J. Magn. Magn Mater. 552 (2022) 169178.
[44] J. Ma, B. Zhao, H. Xiang, F.-Z. Dai, Y. Liu, R. Zhang, et al., High-entropy spinel ferrites MFe_2O_4 (M= Mg, Mn, Fe, Co, Ni, Cu, Zn) with tunable electromagnetic properties and strong microwave absorption, Journal of Advanced Ceramics 11 (5) (2022) 754–768.
[45] B. Omran, K.-H. Baek, Nanoantioxidants: pioneer types, advantages, limitations, and future insights, Molecules 26 (22) (2021) 7031.
[46] K.R. Singh, V. Nayak, J. Singh, A.K. Singh, R.P. Singh, Potentialities of bioinspired metal and metal oxide nanoparticles in biomedical sciences, RSC Adv. 11 (40) (2021) 24722–24746.